Journal of Power Sources 662 (2026) 238755

Contents lists available at ScienceDirect

Journal of Power Sources

journal homepage: www.elsevier.com/locate/jpowsour

Mechanistic insight of Li cluster formation and dendrite deposition in sulfide all-solid-state battery with hard-carbon electrode analyzed using ^{7}Li operando nuclear magnetic resonance

Osamu Tagami [a], Hibiki Fukushima [a], Yumu Nishigaki [a], Ayumi Shikata [b], Masakuni Takahashi [b], Kenjiro Hashi [c], Shinobu Ohki [c], Takashi Teranishi [b], Kazuma Gotoh [a,*]

[a] Center for Nano Materials and Technology (CNMT), Japan Advanced Institute of Science and Technology (JAIST), 1-1 Asahidai, Nomi, Ishikawa, 923-1292, Japan
[b] Graduate School of Natural Science & Technology, Okayama University, 3-1-1 Tsushima-naka, Okayama, 700-8530, Japan
[c] National Institute for Materials Science, 3-13 Sakura, Tsukuba, Ibaraki, 305-0003, Japan

HIGHLIGHTS

- The potential use of hard-carbon for an ASSLB anode was explored using operando NMR.
- Operando ^{7}Li NMR reveals lithium cluster and dendrite behaviors in ASSLBs.
- Quasimetallic Li in open pores or surfaces can induce short-circuits.
- More precise control than liquid LIBs is required to prevent short-circuit.

GRAPHICAL ABSTRACT

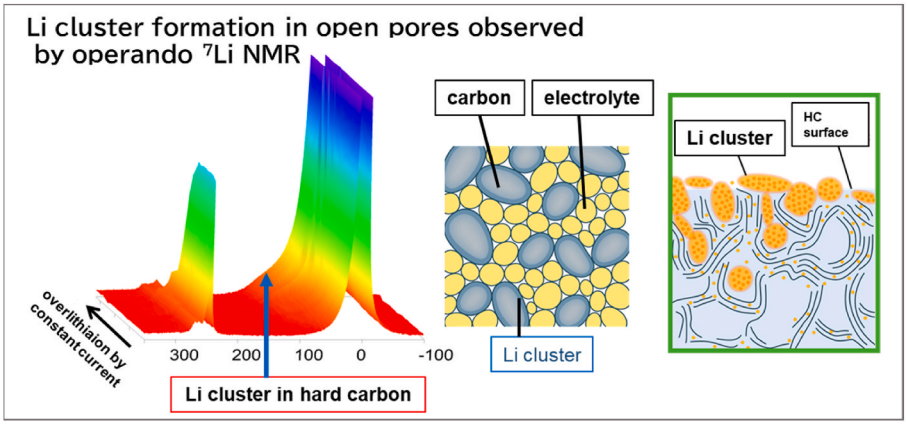

ARTICLE INFO

Keywords:
All solid-state battery
Hard-carbon
Lithium
Solid-state nuclear magnetic resonance
Operando analysis

ABSTRACT

Because lithium dendrite deposition during charging and discharging of all solid-state batteries (ASSLBs) is an important difficulty leading to deactivation, precise analysis of the lithium state is indispensable. We explored the potential use of hard-carbon (HC) for an ASSLB anode using operando ^{7}Li NMR to investigate lithium behavior. Cells using circular electrodes capable of applying constraint pressure to the electrode material were fabricated to achieve precise operando NMR measurements for sulfur-based ASSLBs. Adsorption and desorption behaviors of lithium in HC were found to be nearly identical to those of HC in liquid LIBs. However, short circuits occurred after several hours of constant current overlithiation or potential holding at −5.5 mV although no clear amplification of Li dendrite signal was observed. Signal components attributable to quasimetallic clusters were observed in both cases, which suggests that lithium can form clusters in open pores or on the HC surface during

* Corresponding author.
E-mail address: kgotoh@jaist.ac.jp (K. Gotoh).

https://doi.org/10.1016/j.jpowsour.2025.238755
Received 7 September 2025; Received in revised form 18 October 2025; Accepted 1 November 2025
Available online 7 November 2025

overlithiation. Clusters in the open pores or surface can conduct electricity and may serve as nucleation sites for dendrite growth. Although the use of HC anodes can suppress dendrite formation in ASSLBs, more precise voltage control is required than that used for liquid LIBs.

1. Introduction

Energy storage devices such as secondary batteries, which can store clean energy derived from natural sources, are extremely important for achieving carbon neutrality worldwide. Demand for secondary batteries such as lithium-ion batteries (LIBs) and next-generation batteries is expected to increase considerably, particularly for applications such as electric vehicles (EVs) [1,2]. However, further great advancements in energy density are no longer feasible with current liquid-electrolyte LIBs. Moreover, internal short circuits and cell failures caused by deposition of lithium metal (dendrite) on the negative electrode surface, as well as fires involving organic electrolytes, remain unresolved. All-solid-state lithium-ion batteries (ASSLBs) are currently the most promising candidates to replace solution-based LIBs (liquid LIBs) and polymer-based LIBs [3]. Their safety, which is attributable to the absence of flammable organic electrolytes, is a salient benefit. The superior voltage resistance of solid electrolytes enables much higher energy density than that of liquid LIBs [4,5].

The ionic conductivity of sulfide electrolytes for ASSLB has exceeded 10^{-2} S/cm [6–8], which surpasses that of organic electrolytes [9,10]. Sulfides enable the formation of densely packed electrode materials due to their high plasticity, providing low internal resistance and high energy density (250–500 Wh/kg) [11]. However, many challenges must be overcome before such ASSLBs can be commercialized [12]. In sulfide-based ASSLBs, lithium dendrite formation originates from local inhomogeneities in current density, ionic conductivity, and mechanical contact at the anode–electrolyte interface during lithium deposition. Due to their high ionic conductivity and mechanical plasticity, sulfide electrolytes can relieve local stress while allowing lithium to infiltrate along grain boundaries and structural defects, leading to dendrite channels that penetrate through the electrolyte and reach the cathode, causing short circuits [13]. Insufficient contact between the electrolyte and the negative electrode interface causes current concentration at grain boundaries, leading to dendrite growth [14,15]. This phenomenon is particularly pronounced under high-voltage, high-current operating conditions [16]. It degrades the output characteristics of sulfide-based ASSLBs [17]. Therefore, elucidating the detailed mechanisms of dendrite deposition and short-circuit processes is crucial for the exploration of optimal battery structures capable of suppressing internal short-circuits.

Such state changes in LIBs have been studied using various analytical methods. Ex situ analyses are commonly used to observe state changes before, during, and after charging and discharging, or after overcharging and degradation. Observing the non-equilibrium state during battery operation is also important. Therefore, detailed, real-time operando (in situ) measurements are highly effective for tracking the chemical environmental changes which occur with charging and discharging [18]. In recent years, various operando analysis techniques such as X-ray absorption fine structure analysis (XAFS) [19], X-ray diffraction (XRD) [20,21], electron microscopy [22,23], X-ray CT [24,25], Raman spectroscopy [26], and neutron diffraction [27–30] have been applied for secondary batteries. Nevertheless, these techniques are sometimes not well-suited for the direct observation of dendrites. Since X-ray have difficulty detecting light elements such as Li, analysis and direct detection of Li using XRD or XAFS requires a strong radiation source (synchrotron) [31]. Neutron diffraction excels at obtaining information about the interfaces and structural changes that serve as nucleation sites, rather than depicting the dendrites themselves. Scanning electron microscopy (SEM) cannot provide observations of the electrode interior because it is a surface-scanning technique. It is unable to observe fine lithium particles immediately after formation of crystal or quasi-metallic states. By contrast, solid-state nuclear magnetic resonance (ss-NMR) provides information of the electronic environment surrounding the target nuclei. Therefore, it can distinguish several states of the target nuclei such as ionic lithium compounds, quasimetallic lithium, lithium metal dendrites, and a lithium metal plate of a counter electrode. Several groups, including our group, have conducted research on LIBs and sodium ion batteries (NIBs) using operando or in situ ss-NMR [32–44]. Our group elucidated the mechanisms of dendrite formation on graphite and hard-carbon (HC) electrodes during overcharging of liquid LIBs and NIBs using operando NMR [45]. The study precisely assessed correlation between the onset time of quasimetallic Li/Na or metallic Li/Na deposition and battery potential changes that occurred during the overcharging process. By elucidating the formation mechanisms of quasimetallic and metallic Li/Na during battery overcharging, we estimated the safety limits for overcharging in cells with graphite and HC electrodes.

Operando NMR analysis is also practical for elucidating lithium behavior in ASSLBs. Comparing the behaviors of quasimetallic cluster formation and lithium deposition on carbon electrodes with those of liquid LIBs is extremely valuable for understanding battery characteristics. For this study, we applied operando NMR to sulfide ASSLB and elucidated the Li behaviors in the electrode materials. For the analysis of sulfide-based ASSLBs, operando NMR has been conducted only on symmetric cells [46] or half cells using Li metal electrodes [46,47] to inspect Li-ion transportation and dendrite growth processes during charging and discharging. However, cells using negative electrodes other than Li metal have not been analyzed. For that reason, Li behaviors around negative electrodes remain unclear. In sulfide-based ASSLBs, using a carbon anode rather than lithium metal, other metals (Si, Sn, etc.), or an anode-free type is not only beneficial for preventing Li dendrite deposition and growth. Using a carbon anode is also expected to suppress electrode volume expansion and contraction. Similarly to liquid LIBs, this suppression of volume changes is extremely effective for ensuring battery durability and safety, despite its associated lower capacity when compared to lithium or other metal electrodes. As reported, lithium is stored as a quasimetallic form in HC in liquid LIBs [48–50], which supports higher capacity than graphite. It is fascinating that HC with adequately controlled pore sizes can achieve high capacity in ASSLBs, whereas solution-based LIBs have not. Kaskel et al. reported that the lithiated carbide-derived carbon in an ASSLB with argyrodite electrolyte showed a much larger Knight shift (180 ppm) of quasimetallic Li, which had never been observed in liquid LIBs [51]. In the cells, lithium clusters can be stored not only in closed pores but also in open pores on carbon particle surfaces.

This study was designed to clarify differences in Li behavior during charging and discharging in ASSLBs with an HC anode, and then to compare those findings with those obtained for liquid LIBs. Thereby, the potential of carbon anodes for use in ASSLBs was assessed. To take highly sensitive operando NMR measurements for sulfur-based ASSLBs, cells of two types were fabricated using circular electrodes capable of applying constraint pressure to the electrode material because strong pressurization is required to maintain a contact between electrode particles and electrolyte particles. The charge–discharge and short-circuit processes were observed using these cells.

2. Methods

2.1. Preparation of materials and composite pellets

An argyrodite-type sulfide electrolyte (Li_6PS_5Cl; NEI Corp.) was adopted as the solid electrolyte. As a negative electrode composite material, the electrolyte, an active material (HC), and a conductive additive are used. The electrolyte (Li_6PS_5Cl), HC (Carbotron® PS(F); Kureha Chemical Inds. Corp.), and a conductive additive (VGCF®-H; Resonac Holdings Corp.) were mixed with the weight ratio of 10:6:1, and were ground for 30 min using a mortar and pestle.

A two-layer electrode pellet was prepared, consisting of solid electrolyte and negative electrode compound. First, 60 mg of the Li_6PS_5Cl was pressed at 280 MPa for 5 min in a ϕ8 mm tablet press. After the pressing, 4–5 mg of negative electrode composite was added to one side of the solid electrolyte. After the mixture was pressed at 570 MPa for 10 min, it was molded to a circular shape of ϕ8 mm diameter.

2.2. Assembling cells for operando NMR measurements

To achieve high sealing performance with pressurization functionality within a size to fit inside the NMR probe coil (Fig. 1(a)), we fabricated cell packages of two types made of Poly Ether Ether Ketone (PEEK) body and Cu current collectors. Schematic diagrams and photographs of the cell packages are portrayed respectively in Fig. 1(b) and (c), S1(a) and S1(b). Cell A has a cylindrical outer shape with the electrode disk parallel to the direction of static (external) magnetic field and perpendicular to the radio-frequency pulse irradiated by the NMR solenoid coil (Fig. 1(b) and S1(a)). Cell B, which has similar direction with that of our earlier developed cells [35,45] and commercially available cells [40,52], has its electrode surface oriented as perpendicular to the static magnetic field and parallel to the electromagnetic wave irradiated by the NMR solenoid coil (Fig. 1(b) and S1(a)). The electrodes are not rectangular like those of earlier cells, but are instead disk-shaped to provide uniform pressurization. After cells of both types were assembled, their ^{7}Li NMR spectra were compared. Each PEEK cell was assembled with a Ti foil (ϕ7.8 mm, 0.02 mm thickness), a lithium metal foil as the counter electrode, and a two-layer electrode pellet consisting of the solid electrolyte – negative electrode composite along the direction in which the solid electrolyte contacts the counter electrode. A twist-type lid was then secured. By tightening the lid with a socket wrench, a constraining pressure was applied to the electrolyte inside. The confinement pressure, calculated from the torque and diameter of the screws, was approximately 35 MPa.

The assembled PEEK cells were subjected to charge–discharge testing before operando NMR measurement to confirm their performance. The charge–discharge test of the assembled cells was conducted using a battery charge/discharge system (HJ1001/SD8; Meiden Hokuto Corp.). For comparison, an identical charge–discharge test was conducted using a commercially available metal cell (KP cells; Housen Co. Ltd.). Static ^{7}Li NMR measurements of the assembled PEEK cells were taken to confirm the signal intensity and the peak shift before operando analysis. Each cell for operando NMR was kept at 50 °C throughout the charge–discharge process.

2.3. Operando NMR analyses

Operando ^{7}Li NMR measurements were taken using an NMR spectrometer (AVANCE III 500 MHz; Bruker BioSpin GmbH) equipped with a home-built operando probe (static NMR probe with direct current injection circuit) (Fig. 1(a)). The solenoid coil diameter used for detection was ϕ15 mm to maximize the cell electrode disk size. The coil diameter was almost the maximum size able to fit inside the probe, which can be inserted in the 40 mm inner diameter of the "narrow bore" shim in the NMR magnet. The electrodes in Cell A inserted to the NMR coil were invariably parallel to the external magnetic field, whereas Cell B was placed such that the electrodes were horizontal in the coil. After the electrodes of each cell were connected to a direct current circuit for charging and discharging, ^{7}Li operando NMR measurements were taken. The measurements were performed at 194.4 MHz using a single-pulse sequence. A 1 M LiCl aqueous solution was used as the external standard (0 ppm). The recycling delay and the number of accumulations to obtain one spectrum were set respectively as 5 s and 120. The acquisition to get one spectrum in 5 min was repeated to obtain operando NMR spectra. Every operando NMR measurement was taken at 50 °C. SEM and XPS were performed using TM3030Plus (Hitachi High-Tech Corp.) and KRATOS AXIS-ULTRA DLD (Shimadzu Corp.), respectively.

3. Results and discussion

3.1. Operando cell performance

A typical charge–discharge profile for an operando NMR cell is shown in Fig. S2(a). Cells A and B showed almost identical charge–discharge profiles. The cells were charged and discharged at 50 °C within the range of 2.0 V–0.2 mV. The first discharge (lithiation) was performed using galvanostatic discharge (25 mA g^{-1}) followed by constant-potential discharge (8 h) (CC-CV). Then galvanostatic (CC)

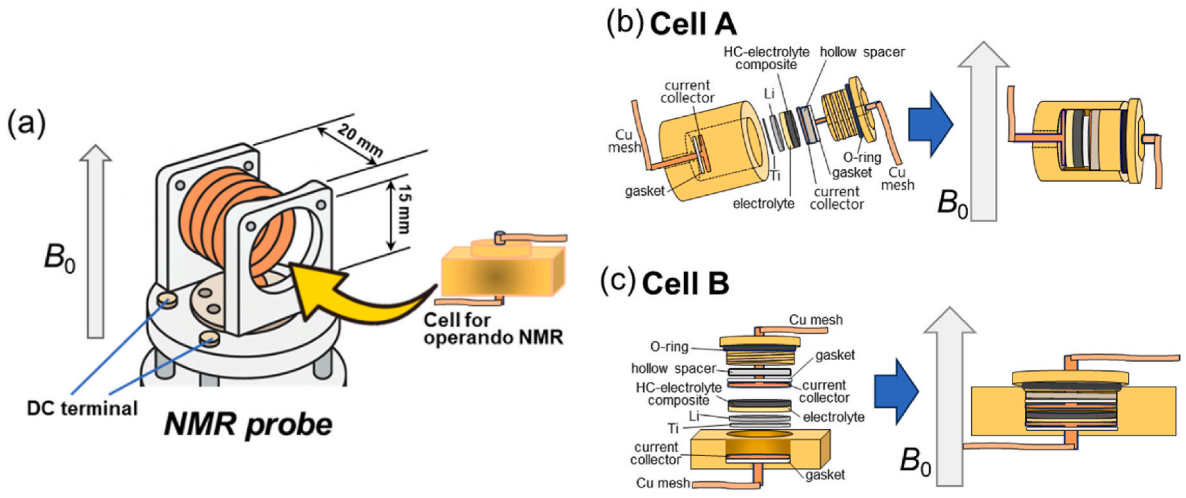

Fig. 1. Structure of the NMR probe head (a) and cells of two types for operando measurement. (b) Cell A: Cylinder-shaped body, electrodes are always parallel to the direction of the static magnetic field. (c) Cell B: Box-shaped body, electrodes are usually installed as perpendicular to the direction of the static magnetic field.

charging and discharging (delithiation) at 25 mA g^{-1} were repeated for two cycles. The first delithiation capacity and the second delithiation capacity were, respectively, 312 and 275 $mAhg^{-1}$, whereas the first and the second delithiation capacities of the commercially available metallic cell were 319 and 289 $mAhg^{-1}$. Those findings indicate clearly that the charge–discharge behavior and capacity are nearly identical. Therefore, the slight capacity decay between the first and second cycles is not attributable to cell design imperfections, but rather to the inherent properties of the cell components: HC and the solid electrolyte. We have reported delithiation capacity of 450 $mAhg^{-1}$ for a liquid LIB using the same HC [48]. Compared to these values, the lower delithiation capacity observed in the solid-state cells examined in this study can be attributed to irreversible side reactions at the interface between the sulfide solid electrolyte and the HC particles. Actually, carbon powder, such as acetylene black, added to the negative electrode can decrease the initial Coulombic efficiency [53].

Fig. 2 and Fig. S3 respectively show an enlarged view and the entire spectra of the ^{7}Li NMR of Cell A and Cell B, assembled respectively using a solid electrolyte – electrode composite and a Li metal counter electrode. In each NMR spectrum, an intense signal corresponding to Li solid electrolyte was observed around 5 ppm. Additionally, signals assigned to the Li counter electrode were confirmed around 260–280 ppm in Cell A and around 245 ppm in Cell B. This peak shift has been attributed to the electrode's anisotropic bulk magnetic susceptibility [54]. The Li electrode signal in Cell B (245 ppm) is an identical peak shift value to our earlier reported rectangular electrode cells [45]. With this configuration, lithium dendrite deposition on the carbon electrode shows the signal at around 275 ppm, making it easy to distinguish between the plate and the dendrite. Furthermore, the higher signal intensity in Cell B than in Cell A enables clearer observation of Li cluster signals in the carbon. Therefore, all subsequent operando NMR measurements were conducted using Cell B.

For operando NMR, assembled pristine cells were pre-discharged at 50 °C to 0.3–0.015 V outside the NMR instrument to save NMR occupation time. State changes caused by charging and discharging (lithiation and delithiation, respectively), and by overdischarging (overlithiation) were observed in the pre-discharged cells.

3.2. Observation of changes accompanying charging and discharging

Fig. 3 shows the discharge–charge profile of an assembled cell (Fig. 3 (a)) and the corresponding operando ^{7}Li NMR spectra (Fig. 3(b) and (c)). The cell was lithiated galvanostatically at 25 mAh g-1 from 0.3 V to the termination potential at 0.2 mV. After the potential reached 0.2 mV at 10.8 h following the start of lithiation, the process was switched to CV lithiation for 5.5 h at 0.2 mV. Subsequently, galvanostatical delithiation at 50 mAh g-1 was applied up to 1.8 V. Delithiation was started from 16.3 h and was continued until 22 h later, but a voltage disturbance thought to be caused by a partial internal short circuit started from 1.7 V. In the corresponding operando ^{7}Li NMR spectra (Fig. 3(b)), signals of Li ions in the solid electrolyte (SE) near 3 ppm and of Li metal of the counter electrode (Li CE) (240–270 ppm) were observed throughout measurements. In this cell, the Li CE signal shows a main component at 245 ppm and a minor peak at 272 ppm. Although the peak value of the latter peak corresponds to the dendrite signal, the peak is unlikely to be associated with the dendrite formation from the start of delithiation. Rather, it is a deformed structure of counter electrode parallel to the static magnetic field created by the strong confinement pressure. During the lithiation process, a new peak began to appear on the higher-frequency side (10–50 ppm) of the SE signal at approximately 8.7 h, after the potential dropped below 13 mV. Even after the transition to CV process, the peak (Li HC) continued to shift toward higher frequencies while increasing in intensity. At the end of lithiation (16.3 h), the peak shifted to 91 ppm. In the subsequent delithiation, this peak shifted rapidly to the lower frequency side and disappeared at 0.2 V of the potential. The peak behavior is attributable to the formation and dissipation of quasimetallic lithium clusters in the HC. Although quasimetallic lithium species have been observed in amorphous carbon electrodes with an argyrodite type solid electrolyte system using ex situ NMR in an earlier study [51], our experiment is the first successful direct observation of the formation and disappearance process of quasimetallic lithium using operando NMR. Similarly to the results of the liquid LIBs' analysis, the NMR peak shifted gradually, indicating that lithium clusters grew gradually with current application. Additionally, the peak intensity of Li at around 275 ppm remained almost unchanged during lithiation and delithiation, which indicates that dendrite deposition occurred only slightly. Furthermore, the signal at 245 ppm is nearly constant during lithiation, except for a slight decrease after the first 3 h. It also decreased during partial short-circuiting at the end of delithiation (Fig. 3(c)). This decrease suggests that the Li which emerged from the carbon electrode during charging does not return to its original plate form. This lack of reversion is likely to be attributable to gradual dissolution of the Li metal electrode caused by the strong current flow which occurs during short-circuiting.

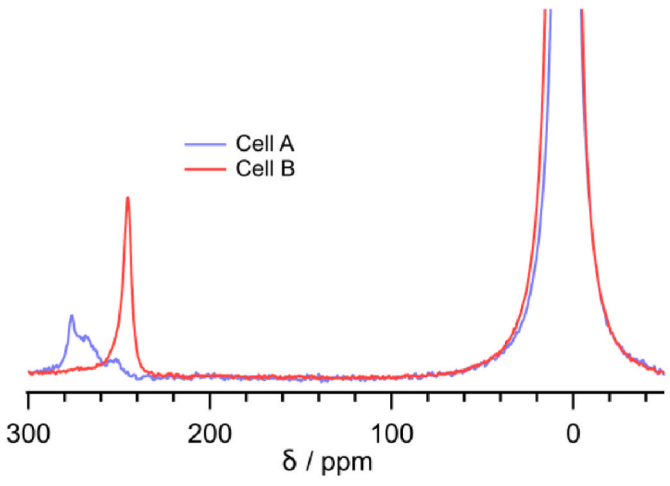

Fig. 2. Enlarged ^{7}Li NMR spectra of Cell A and Cell B assembled using solid electrolyte – electrode composite and Li metal counter electrodes (Complete spectra are in Fig. S3.).

3.3. Observation of the overlithiation process associated with continuous CC discharge

Fig. 4 shows the operando ^{7}Li NMR spectrum obtained by overlithiation without setting a lower limit potential using Cell B. The prelithiated cell at 0.03 V was discharged at 50 mA g^{-1}. The potential decreased rapidly at first and dropped below 0 V. Then the rate slowed. After the potential reached a minimum at −20 mV after 50 min, the potential remained nearly constant for approximately 1 h. During that process, a very weak signal corresponding to quasimetallic Li clusters in the HC (Li HC) at approximately 80 ppm was observed immediately after the potential dropped below 0 V. The maintained potential began to decay considerably after 2 h, and eventually reached −0.22 V. Then a sudden voltage rise and subsequent disturbance attributable to a partial internal short circuit occurred. Interestingly, the signal intensity of the counter electrode Li began to decrease after 1.5 h, and most of them disappeared by 2.5 h. Although it is difficult to provide a clear explanation for the detailed cause of such a sudden rapid decrease, the unstable condition inside the cell at negative potential might accelerate the melting of the Li metal counter electrode and a short circuit on the carbon electrode side. During the potential decrease from 2.0 h and short circuit after 3.0 h, the signal of the quasimetallic clusters increased. Because the apparent metal dendrite signal was not observed by NMR, it is possible that accumulation of quasimetallic clusters might increase the conductivity on the negative electrode side.

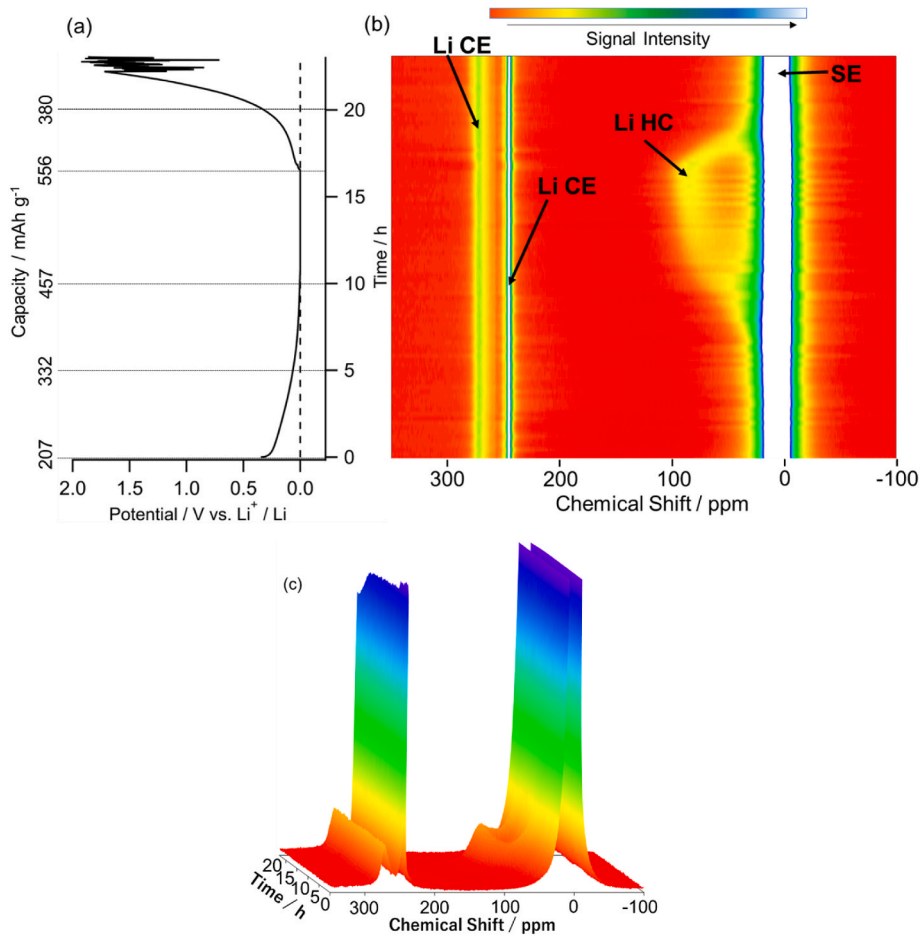

Fig. 3. The 1st cycle of the discharge–charge profile of an assembled cell (a), and the corresponding operando ^{7}Li NMR spectra (b)(c).

We conducted similar experiments using a cell with lower confinement pressure (less than 10 MPa) (Fig. S4). In this cell, quasimetallic Li signal was not observed through the overlithiation, whereas the dendrite signal appeared and increased at 278 ppm after 1.7 h. The electric potential showed no minimum value. During lithiation, the cell had a potential plateau at around −0.1 V at once. Then a further potential drop occurred from the onset of dendrite deposition. Finally, a short circuit occurred at 3.1 h. Effective contact between negative electrode particles or between solid electrolyte particles is not maintained if the confinement pressure is insufficient, resulting in inefficient Li insertion into the carbon. Therefore, Li is not stored into carbon as a cluster but is deposited as a dendrite on carbon particle surfaces or among carbon particles and solid electrolyte particles, which grow and apparently lead to short circuits in the cell.

From an earlier study, we observed that dendritic lithium begins to form after the growth of quasimetallic lithium clusters in liquid LIB during overlithiation [45]. This formation of quasimetallic lithium clusters is expected to have an inhibitory effect on dendritic lithium formation in liquid LIB. In ASSLBs subjected to overlithiation measurements, this buffering effect was much weaker than in the solution system. In a liquid LIB, the potential remained at −50 mV for over 5 h without a short circuit at an overlithiation rate of 0.4 C. In the solution cells, cluster lithium formation occurs exclusively within the internal closed pores of HC, to which an electrolyte solution cannot access. Such lithium clusters in these internal closed pores neither trigger dendrite formation nor contribute to growth. The lithium atoms constituting the lithium clusters exist as ions with a certain valence, unlike the dendrite which has completely zero-valent metals. Consequently, the clusters react more easily with the organic solvent than with zero-valent metal particles. By contrast, clusters can be formed in the open pores or on the surface of the HC in ASSLBs. Their formation is energetically easier than dendrite formation where there is no reaction with the electrolyte. Even if explicit metal dendrite formation does not occur, cluster formation in the open pores or on the surface might have created conductive paths leading to local short circuits. To verify this hypothesis further, we conducted the experiment described below, for which the cell was maintained at a constant potential of −5.5 mV.

3.4. State change caused by leaving a negative potential

Kaskel et al. reported that lithium metal plating is observed at potential greater than 5.0 mV when a symmetric cell using an argyrodite-type electrolyte was charged and discharged [51]. According to those findings, to investigate the presence or absence of dendrite deposition, we maintained the operando cell kept at −5.5 mV, which is just the potential at which lithium plating is likely to occur. Before the operando experiment, Cell B was lithiated to 15 mV at 25 mAh g^{-1} outside the NMR. Then the cell was lithiated to −5.5 mV at 25 mAh g^{-1} and held at −5.5 mV. The profile and the corresponding operando NMR spectra are presented in Fig. 5. At the start of NMR measurement, a signal of quasimetallic lithium clusters at 74 ppm was confirmed. The cell reached the −5.5 mV immediately upon the start of lithiation. Subsequently, the Li HC signal intensity increased and became very clear with lithiation, shifting to 98 ppm over time. During the subsequent potential holding, no marked change in the peak shift of the cluster state was observed, although its signal intensity increased gradually. In addition, the formation of lithium dendrites was not detected clearly. The cell finally reached a total short circuit at 10.8 h. The signals corresponding to

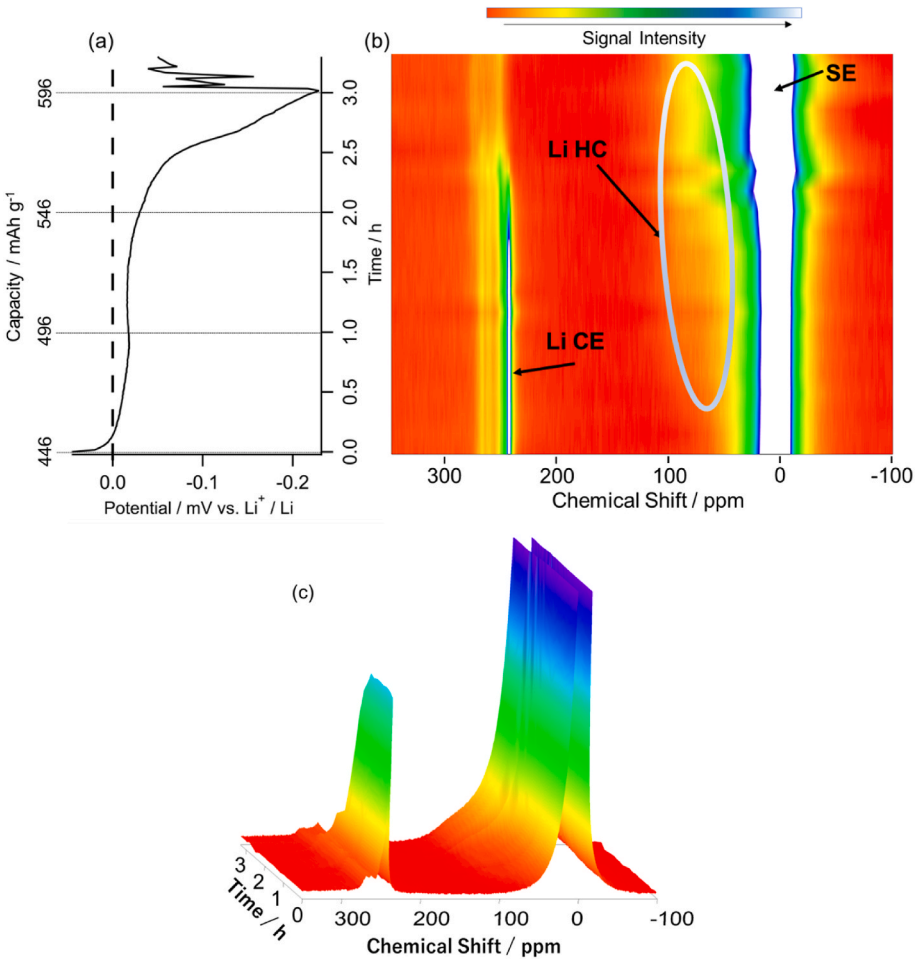

Fig. 4. The operando ^{7}Li NMR spectrum obtained by overlithiation without setting a lower limit potential using Cell B. The pre-lithiated cell at 0.03 V was discharged at 50 mA g^{-1}. (a) profile of an assembled cell, (b)(c) the corresponding operando ^{7}Li NMR spectra.

lithium counter electrodes and dendrites increased rapidly after the short circuit, which indicates dendrite formation on the current path and on the counter electrode surface. We reported that continued lithiation at a negative potential is possible for some time in the liquid LIBs, even if dendrites form to a certain extent. However, by contrast, a short circuit can occur even after prolonged holding at a constant negative potential of −5.5 mV in solid electrolyte cells. In spite of the absence of clear dendrite formation and growth during the process in NMR observation, short circuit can be led finally at the negative potential, which suggests that minute dendrites may have rapidly formed and grown, leading to short circuits. Therefore, we fabricated the cell again under the same conditions, then maintained it at −5.5 mV for 10 h after CC lithiation. The cell was disassembled, and the electrode was extracted for SEM observation and XPS measurement.

In SEM observations, the surfaces of the electrode-electrolyte interphase layer were compared between pristine samples and samples after discharging (after constant-potential holding at −5.5 mV for 10 h). Since the apparatus for non-exposed atmospheric measurements could not be used, the metallic lithium had already decomposed, making observation of the Li metal impossible. However, in the post-discharge samples, an obvious increase in cracks on the surfaces was observed. Also, a substance that may be dendritic decomposition products is present on the surface of the sample after discharge (Fig. S5).

XPS measurements were also performed after short-time atmospheric exposure when the sample was placed inside the apparatus (Fig. S6). No significant spectral changes were observed for P (2p) and S (2p), indicating no major state changes in the electrolyte. This result is similar to existing XPS observations of air-exposed Li_6PS_5Cl [55]. In contrast, the C (1s) spectra exhibited a significant change in shape. This indicates that most of the C atoms on the surface of hard carbon reacted with lithium during discharge. The main peak at 284.2 eV is likely representing C-O, which was created by the decomposition of Li-bonded C, whereas a minor peak at 288.2 eV can be ascribed to C=O [56,57]. It is possible that dendrites of sub-nanometer size, which are almost undetectable by NMR, grew to trigger a short circuit in the electrolyte layer.

3.5. *Mechanisms of cluster formation, dendrite precipitation, and short circuits*

During constant current overlithiation or when keeping negative potential of the cells, lithium ion is supplied continuously from the counter electrode to the working (HC) electrode. In liquid LIBs, both constant current overlithiation and constant voltage holding first result in cluster formation [45]. In both cases, the shift values exceed 100 ppm. The cluster signal intensity is also clear. The intensity indicates that sufficient Li insertion and cluster formation occur within the closed pores of the HC. Dendrite deposition on the HC surface begins after the internal pore space is filled. A considerable amount of time is necessary for dendrite formation on the carbon surface in the electrolyte solution. The connection of dendrites on adjacent particles ultimately leads to a short circuit. By comparison, clusters also form both during constant current overlithiation and during constant voltage holding in the solid electrolyte. However, the clusters formed during constant current

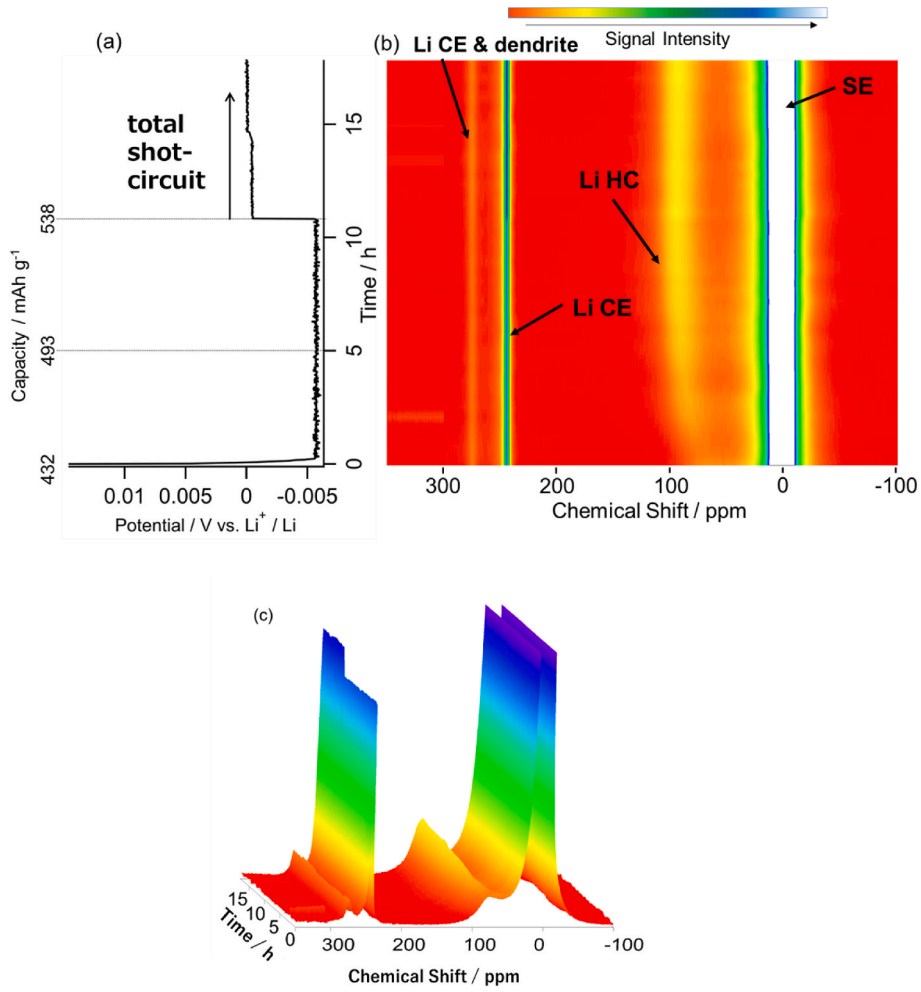

Fig. 5. Operando ^{7}Li NMR spectra of over-lithiated cell. Then the cell was lithiated from 15 mV to −5.5 mV at 25 mAhg^{-1}. The potential was kept at −5.5 mV. (a) profile of an assembled cell, (b)(c) the corresponding operando ^{7}Li NMR spectra.

overlithiation are markedly fewer than those formed during constant voltage holding. The clusters formed during constant voltage holding are roughly equivalent to those formed in solution batteries. In solid-state batteries, no great difference exists in the ease of Li cluster formation between the closed pores inside the HC and the open pores on the surface because there is no solvent. With constant current overlithiation, cluster growth over time inside the pores is less likely to occur than with constant voltage holding. Cluster formation on the HC particle surface, where Li is supplied immediately from the outside, occurs preferentially.

Direct structural analysis of Li clusters using XRD is impossible to support this discussion completely. However, for Na clusters formed in the HC anodes of Na-ion batteries through electrochemical insertion with a mechanism similar to Li, Pair Distribution Function (PDF) analysis of XRD has been conducted by Stratford et al. [58]. According to their report, sodium in fully sodiated HC, forming sodium metal nanoclusters, has size of 1.2–1.5 nm. The quasimetallic clusters observed by NMR are understood as fine metal particles in PDF analysis. Their electronic conductivity is predicted to be high, even if not equivalent to that of sodium metal. As with sodium clusters, lithium clusters are also expected to have high conductivity. The clusters might not exhibit the same Knight shift as bulk metal in NMR measurements because the number of conductive electrons in the clusters is not as high as in metal. Additionally, the average shift toward lower frequencies caused by exchange with interlayer Li ions might produce a peak of approximately 100 ppm. However, the clusters are fundamentally highly conductive, similar to bulk Li metal, and might contribute to short circuits. Furthermore, clusters formed in the open pores on the HC surface may also serve as nucleation sites for dendrite growth. A schematic diagram of the state of the electrode composite based on the discussion is presented in Fig. 6.

For this study, charging and discharging of the cells for operando measurement were conducted at 50 °C, at which temperature lithium moves more easily in the electrolyte than at room temperature. However, because ASSLBs exhibit further increases in conductivity and show favorable Li diffusion at high temperatures, operando NMR measurements at higher temperatures can support observation of cluster and dendrite formation mechanisms under various conditions, potentially elucidating battery characteristics. The cells fabricated for this study were designed to withstand temperatures of approximately 150 °C. However, when actually conducting experiments at high temperatures, marked degradation of the battery components (electrolyte, counter electrode, and Li-doped carbon) was observed inside the cells. Charging and discharging did not occur properly, probably because of the great increase in the nitrogen gas and water vapor permeability of the PEEK body at high temperatures. By preparing cells that maintain excellent gas barrier properties at high temperatures and which can withstand applied pressure, we anticipate that high-temperature measurements of ASSLBs can be achieved in future studies.

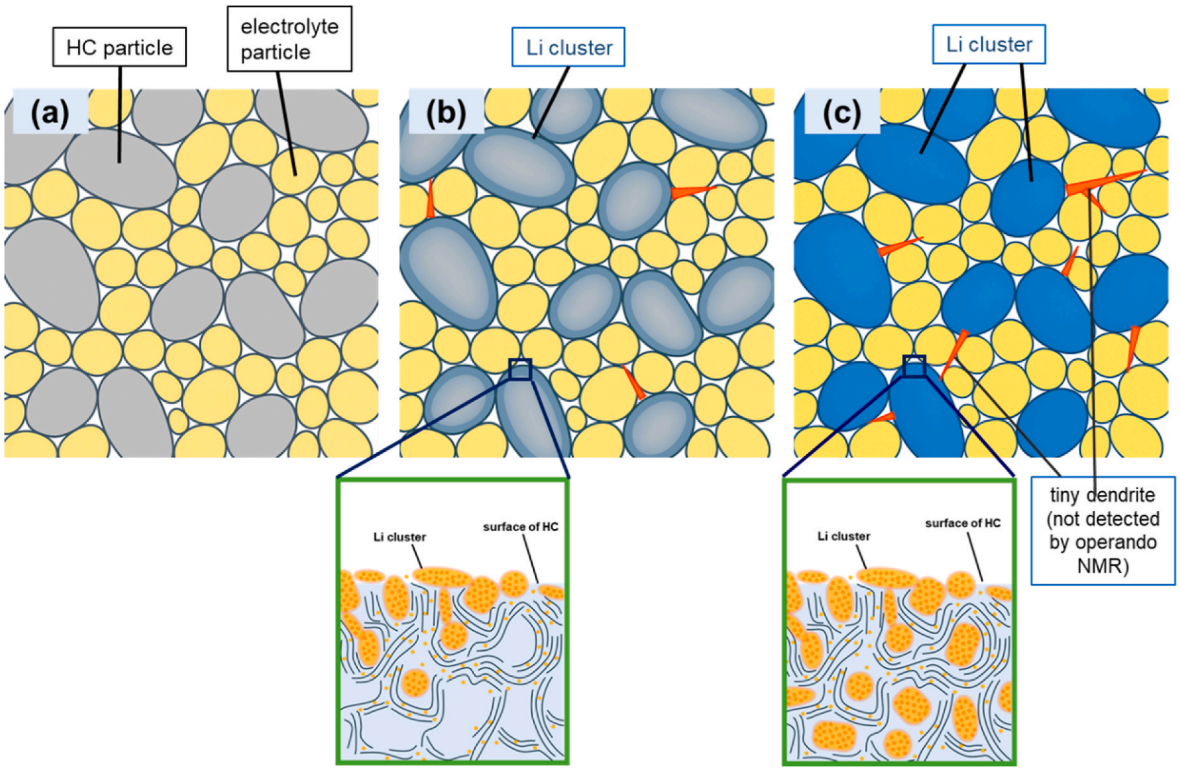

Fig. 6. Schematic diagram of structural changes in the negative electrode composite material. (a) Before electrochemical lithium introduction. (b) During Li over-insertion at a constant current. Lithium clusters are adsorbed on HC particle surfaces or in open pores near the surface, forming quasimetallic clusters (dark gray areas on the HC surface in the figure). (c) State after a holding test at −5.5 mV. Lithium clusters are generated not only on the HC particle surfaces and in open pores but also in closed pores (blue regions within HC particles). Tiny dendrites that were not observed in operando NMR due to overlapping of the counter electrode signal can assist in short-circuiting. Attention should be paid that although these figures do not show the conductive additive, it can also contribute to formation of short-circuit paths among HC particle surfaces. (For interpretation of the references to colour in this figure legend, the reader is referred to the Web version of this article.)

4. Conclusion

We performed operando NMR evaluation of sulfide ASSLBs using HC anodes. By assembling a half-cell using a cell case that allows application of constraint pressure via screws, sensitive detection of the signal of lithium clusters in HC and precise observation of lithium dendrite deposition were realized.

Cluster formation and decomposition processes with lithiation and delithiation were observed using ^{7}Li operando NMR. Adsorption and desorption behaviors of lithium in the HC are nearly identical to those of HC in liquid LIBs during discharge and subsequent charging between 2 V and 0 V. However, in CC overdischarge and −5.5 mV hold experiments, short circuits respectively occurred after 3 h and 10 h, although no clear amplification of Li dendrite signals was observed. Instead, signal components attributable to quasimetallic clusters were observed in both cases. These findings suggest that lithium can form clusters in the open pores or on HC surfaces during overlithiation. Such clusters can conduct electricity and may serve as nucleation sites for dendrite growth. Additionally, holding the potential at negative strongly facilitates cluster formation within the closed pores through slow lithiation. In liquid LIBs, clusters do not form in open pore space. During overdischarge of HC in liquid LIBs, cluster formation occurs preferentially over dendrite formation, rendering the cell resistant to overcharging. In solid electrolyte batteries, a short circuit occurring before apparent dendrite formation makes it more difficult to ascertain the safety limit of the battery. Preventing short circuits in solid state batteries demands more precise voltage management and control than for solution cells.

CRediT authorship contribution statement

Osamu Tagami: Writing – original draft, Validation, Methodology, Conceptualization. **Hibiki Fukushima:** Formal analysis, Data curation. **Yumu Nishigaki:** Visualization, Data curation. **Ayumi Shikata:** Methodology. **Masakuni Takahashi:** Resources, Investigation. **Kenjiro Hashi:** Methodology, Data curation. **Shinobu Ohki:** Resources, Data curation. **Takashi Teranishi:** Validation. **Kazuma Gotoh:** Writing – original draft, Supervision, Project administration, Funding acquisition, Conceptualization.

Declaration of competing interest

The authors declare that they have no known competing financial interests or personal relationships that could have appeared to influence the work reported in this paper.

Acknowledgement

This work was supported by JSPS KAKENHI Grant No. 23K04535, 24K01162, and ATLA Grant No. JPJ004596. The homebuilt NMR probe was fabricated at Probe Lab. Inc. XPS measurements and SEM observations were supported respectively by Mr. Tatsuya Murakami and Mr. Koichi Higashimine in Center of Nano Materials and Technology, JAIST.

Appendix B. Supplementary data

Supplementary data to this article can be found online at https://doi.org/10.1016/j.jpowsour.2025.238755.

Data availability

Data will be made available on request.

References

[1] J.M. Tarascon, M. Armand, Issues and challenges facing rechargeable lithium batteries, Nature 414 (6861) (2001) 359–367, https://doi.org/10.1038/35104644.

[2] L. Lu, X. Han, J. Li, J. Hua, M. Ouyang, A review on the key issues for lithium-ion battery management in electric vehicles, J. Power Sources 226 (2013) 272–288, https://doi.org/10.1016/j.jpowsour.2012.10.060.

[3] M. Tatsumisago, M. Nagao, A. Hayashi, Recent development of sulfide solid electrolytes and interfacial modification for all-solid-state rechargeable lithium batteries, J. Asian Ceram. Soc. 1 (2013) 17–25, https://doi.org/10.1016/j.jascer.2013.03.005.

[4] G. Zubi, R. Dufo-López, M. Carvalho, G. Pasaoglu, The lithium-ion battery: state of the art and future perspectives, Renew. Sustain. Energy Rev. 89 (2018) 292–308, https://doi.org/10.1016/j.rser.2018.03.002.

[5] Q. Zhao, S. Stalin, C.Z. Zhao, L.A. Archer, Designing solid-state electrolytes for safe, energy-dense batteries, Nat. Rev. Mater. 5 (3) (2020) 229–252, https://doi.org/10.1038/s41578-019-0165-5.

[6] J. Li, Y. Li, S. Zhang, T. Liu, D. Li, L. Ci, Long cycle life all-solid-state batteries enabled by solvent-free approach for sulfide solid electrolyte and cathode films, Chem. Eng. J. 455 (2023) 140605, https://doi.org/10.1016/j.cej.2022.140605.

[7] J.C. Wang, P.F. Wang, T.F. Yi, Challenges and optimization strategies at the interface between sulfide solid electrolyte and lithium anode, Energy Storage Mater. 62 (2023) 102958, https://doi.org/10.1016/j.ensm.2023.102958.

[8] J. Wu, S. Liu, F. Han, X. Yao, C. Wang, Lithium/sulfide all-solid-state batteries using sulfide electrolytes, Adv. Mater. 33 (2021) 2000751, https://doi.org/10.1002/adma.202000751.

[9] N. Kamaya, K. Homma, Y. Yamakawa, M. Hirayama, R. Kanno, M. Yonemura, T. Kamiyama, Y. Kato, S. Hama, K. Kawamoto, A. Mitsui, A lithium superionic conductor, Nat. Mater. 10 (2011) 682–686, https://doi.org/10.1038/nmat3066.

[10] Y. Kato, S. Hori, T. Saito, K. Suzuki, M. Hirayama, A. Mitsui, M. Yonemura, H. Iba, R. Kanno, High-power all-solid-state batteries using sulfide superionic conductors, Nat. Energy 1 (2016) 16030, https://doi.org/10.1038/nenergy.2016.30.

[11] W.G. Suci, H.K. Aliwarga, Y.R. Azinuddin, R.B. Setyawati, K.N.R. Stulasti, A. Purwanto, Review of various sulfide electrolyte types for solid-state lithium-ion batteries, Open Eng. 12 (2022) 409–423, https://doi.org/10.1515/eng-2022-0043.

[12] Q. Zhang, D. Cao, Y. Ma, A. Natan, P. Aurora, H. Zhu, Sulfide-based solid-state electrolytes: synthesis, stability, and potential for all-solid-state batteries, Adv. Mater. 31 (2019) 1901131, https://doi.org/10.1002/adma.201901131.

[13] D.K. Singh, A. Henss, B. Mogwitz, B. Mogwitz, A. Gautam, J. Horn, T. Krauskopf, S. Burkhardt, J. Sann, F.H. Richter, J. Janek, Li_6PS_5Cl microstructure and influence on dendrite growth in solid-state batteries with lithium metal anode, Cell Rep. Phys. Sci. 3 (2022) 101043, https://doi.org/10.1016/j.xcrp.2022.101043.

[14] R. Guo, K. Zhang, W. Zhao, Z. Hu, S. Li, Y. Zhong, R. Yang, X. Wang, J. Wang, C. Wu, Y. Bai, Interfacial challenges and strategies toward practical sulfide-based solid-state lithium batteries, Energy Mater. Adv. 4 (2023) 22, https://doi.org/10.34133/energymatadv.0022.

[15] S. Luo, Z. Wang, X. Li, X. Liu, H. Wang, W. Ma, L. Zhang, L. Zhu, X. Zhang, Growth of lithium-indium dendrites in all-solidstate lithium-based batteries with sulfide electrolytes, Nat. Commun. 12 (2021) 6968, https://doi.org/10.1038/s41467-021-27311-7.

[16] J. Hu, S. Yang, Y. Pei, X. Wang, Y. Liao, S. Li, A. Yue, J.-Q. Huang, H. Yuan, Perspective on powder technology for all-solid-state batteries: how to pair sulfide electrolyte with high-voltage cathode, Particuology 86 (2024) 55–66, https://doi.org/10.1016/j.partic.2023.04.005.

[17] D.K. Singh, T. Fuchs, C. Krempaszky, B. Mogwitz, J. Janek, Non-linear kinetics of the lithium metal anode on Li_6PS_5Cl at high current density: dendrite growth and theRole of lithium microstructure on creep, Adv. Sci. 10 (2023) 2302521, https://doi.org/10.1016/j.partic.2023.04.005.

[18] P.P.R.M.L. Harks, F.M. Mulder, P.H.L. Notten, In situ methods for Li-ion battery research: a review of recent developments, J. Power Sources 288 (2015) 92–105, https://doi.org/10.1016/j.jpowsour.2015.04.084.

[19] M.G. Giuliana Aquilanti, Robert Dominko, Lorenzo Stievano, Iztok Arčon, Nicola Novello, Luca Olivi, Operando characterization of batteries using x-ray absorption spectroscopy: advances at the beamline XAFS at synchrotron elettra, J. Phys. D Appl. Phys. 50 (2017) 074001, https://doi.org/10.1088/1361-6463/aa519a.

[20] N. Ishida, Y. Saito, K. Okada, A. Shintani, K. Sugiura, M. Kawai, K. Kawamoto, Operando XRD analysis of self-discharge induced by elevated temperature for sulfide-based all-solid-state Li-ion batteries, J. Power Sources 652 (2025), https://doi.org/10.1016/j.jpowsour.2025.237577.

[21] Y. Takabayashi, K. Kimura, T. Miyazaki, K. Yoshii, H. Sakaebe, M. Shikano, N. Takeichi, T. Nakatani, S. Fujinami, H. Kiuchi, M. Katayama, T. Hirano, K. Hayashi, Operando combined SAXS/XRD/XAFS measurements of lithium conversion battery, Adv. Sust. Syst. 8 (2024) 2300571, https://doi.org/10.1002/adsu.202300571.

[22] S. Tao, M. Li, M. Lyu, L. Ran, R. Wepf, I. Gentle, R. Knibbe, In operando closed-cell transmission electron microscopy for rechargeable battery characterization: scientific breakthroughs and practical limitations, Nano Energy 96 (2022), https://doi.org/10.1016/j.nanoen.2022.107083.

[23] G. He, Y. Oshima, M. Tomitori, In-situ high-resolution scanning electron microscopy observation of electrodeposition and stripping of lead in an electrochemical cell, Jpn. J. Appl. Phys. 60 (2021) 035509, https://doi.org/10.35848/1347-4065/abe640.

[24] D.P. Finegan, M. Scheel, J.B. Robinson, B. Tjaden, I. Hunt, T.J. Mason, J. Millichamp, M. Di Michiel, G.J. Offer, G. Hinds, D.J.L. Brett, P.R. Shearing, In-operando high-speed tomography of lithium-ion batteries during thermal runaway, Nat. Commun. 6 (2015) 6924, https://doi.org/10.1038/ncomms7924.

[25] M. Ebner, F. Marone, M. Stampanoni, V. Wood, Visualization and quantification of electrochemical and mechanical degradation in li ion batteries, Science 342 (2013) 716–720, https://doi.org/10.1126/science.1241882.

[26] Y. Ito, C. Lee, Y. Miyahara, K. Miyazaki, T. Abe, Operando raman spectroscopy insights into the electrochemical formation of F-Graphite intercalation compounds, ACS Energy Lett. 9 (2024) 1473–1479, https://doi.org/10.1021/acsenergylett.4c00130.

[27] G. Liang, C. Didier, Z. Guo, W.K. Pang, V.K. Peterson, Understanding rechargeable battery function using in operando neutron powder diffraction, Adv. Mater. 32 (2020) 1904528, https://doi.org/10.1002/adma.201904528.

[28] L. Vitoux, M. Reichardt, S. Sallard, P. Novák, D. Sheptyakov, C. Villevieille, A cylindrical cell for operando neutron diffraction of Li-ion battery electrode materials, Front. Energy Res. 6 (2018) 00076, https://doi.org/10.3389/fenrg.2018.00076.

[29] O. Korjus, S. Anil Kumar, L. Grendrin, S. Vial, C. Villevieille, E. Suard, Enabling operando neutron diffraction for solid-state battery studies, ACS Mater. Lett. 7 (2025) 2725–2731, https://doi.org/10.1021/acsmaterialslett.5c00596.

[30] F. Han, A.S. Westover, J. Yue, X. Fan, F. Wang, M. Chi, D.N. Leonard, N.J. Dudney, H. Wang, C. Wang, Nat. Energy 4 (2019) 187–196, https://doi.org/10.1038/s41560-018-0312-z.

[31] Z. Ning, D.S. Jolly, G. Li, R.D. Meyere, S.D. Pu, Y. Chen, J. Kasemchainan, J. Ihli, C. Gong, B. Liu, D.L.R. Melvin, A. Bonnin, O. Magdysyuk, P. Adamson, G. O. Hartley, C.W. Monroe, T.J. Marrow, P.G. Bruce, Visualizing plating-induced cracking in lithium-anode solid-electrolyte cells, Nat. Mater. 20 (2021) 1121–1129, https://doi.org/10.1038/s41563-021-00967-8.

[32] M. Letellier, F. Chevallier, C. Clinard, E. Frackowiak, J.-N. Rouzaud, F. Beguin, M. Morcrette, J.-M. Tarascon, The first in situ ^{7}Li nuclear magnetic resonance study of lithium insertion in hard-carbon anode materials for Li-ion batteries, J. Chem. Phys. 118 (2003) 6038–6045, https://doi.org/10.1063/1.1556092.

[33] M. Letellier, F. Chevallier, M. Morcrette, In situ ^{7}Li nuclear magnetic resonance observation of the electrochemical intercalation of lithium in graphite: first cycle, Carbon 45 (2007) 1025–1034, https://doi.org/10.1016/j.carbon.2006.12.018.

[34] F. Blanc, M. Leskes, C.P. Grey, In situ solid-state NMR spectroscopy of electrochemical cells: batteries, supercapacitors, and fuel cells, Acc. Chem. Res. 46 (2013) 1952–1963, https://doi.org/10.1021/ar400022u.

[35] K. Gotoh, M. Izuka, J. Arai, Y. Okada, T. Sugiyama, K. Takeda, H. Ishida, In situ ^{7}Li nullear magnetic resonance study of the relaxation effect in practical lithium ion batteries, Carbon 79 (2014) 380–387, https://doi.org/10.1016/j.carbon.2014.07.080.

[36] K. Shimoda, M. Murakami, D. Takamatsu, H. Arai, Y. Uchimoto, Z. Ogumi, In situ NMR observation of the lithium extraction/insertion from $LiCoO_2$ cathode, Electrochim. Acta 108 (2013) 343–349, https://doi.org/10.1016/j.electacta.2013.06.120.

[37] O. Pecher, J. Carretero-Gonzalez, K.J. Griffith, C.P. Grey, Materials' methods: NMR in battery research, Chem. Mater. 29 (2017) 213–242, https://doi.org/10.1021/acs.chemmater.6b03183.

[38] S. Wiemers-Meyer, M. Winter, S. Nowak, A battery cell for in situ NMR measurements of liquid electrolytes, Phys. Chem. Chem. Phys. 19 (2017) 4962–4966, https://doi.org/10.1039/C6CP08653E.

[39] S.A. Kayser, A. Mester, A. Mertens, P. Jakes, R.-A. Eichel, J. Granwehr, Long-run in operando NMR to investigate the evolution and degradation of battery cells, Phys. Chem. Chem. Phys. 20 (2018) 13765–13776, https://doi.org/10.1039/C8CP01067F.

[40] K. Märker, C. Xu, C.P. Grey, Operando NMR of NMC811/Graphite lithium-ion batteries: structure, dynamics, and lithium metal deposition, J. Am. Chem. Soc. 142 (2020) 17447–17456, https://doi.org/10.1021/jacs.0c06727.

[41] K.J. Sanders, A.R. Aguilera, J.R. Keffer, B.J. Balcom, I.C. Halalay, G.R. Goward, Transient lithium metal plating on graphite: operando ^{7}Li nullear magnetic resonance investigation of a battery cell using a novel RF probe, Carbon 189 (2022) 377–385, https://doi.org/10.1016/j.carbon.2021.12.082.

[42] H. Fujimoto, K. Shimoda, M. Murakami, H. Kiuchi, S. Takagi, G. Kano, M. Kawasaki, Z. Ogumi, T. Abe, In-Plane ordering of Li-Intercalated turbostratic graphite for the negative electrode of high-power long-life Li-Ion batteries, J. Electrochem. Soc. 170 (2023) 060534, https://doi.org/10.1149/1945-7111/acde63.

[43] M. Gabrijelčič, B. Tratnik, G. Kapun, E. Tchernychova, N. Zabukovec Logar, A. Krajnc, R. Dominko, A. Vizintin, Probing sodium structures and dynamics in hard carbon for Na-ion batteries using ^{23}Na operando solid-state NMR spectroscopy, J. Mater. Chem. A 13 (2025) 1042–1056, https://doi.org/10.1039/D4TA07135B.

[44] K. Gotoh, ^{23}Na solid-state NMR analyses for Na-Ion batteries and materials, Batter. Supercaps 4 (2021) 1267–1278, https://doi.org/10.1002/batt.202000295.

[45] K. Gotoh, T. Yamakami, I. Nishimura, H. Kometani, H. Ando, K. Hashi, T. Shimizu, H. Ishida, Mechanisms for overcharging of carbon electrodes in lithium-ion/sodium-ion batteries analysed by operando solid-state NMR, J. Mater. Chem. A 8 (2020) 14472–14481, https://doi.org/10.1039/D0TA04005C.

[46] Z. Liang, Y. Xiang, K. Wang, J. Zhu, Y. Jin, H. Wang, B. Zheng, Z. Chen, M. Tao, X. Liu, Y. Wu, R. Fu, C. Wang, M. Winter, Y. Yang, Understanding the failure process of sulfide-based all-solid-state lithium batteries via operando nuclear magnetic resonance spectroscopy, Nat. Commun. 14 (2023) 259, https://doi.org/10.1038/s41467-023-35920-7.

[47] X. Chen, J. Zhang, G. Zhong, Y. Ouyang, S. Yu, C. Wang, K. Sun, X. Liao, X. Kuang, Y. Chen, Z. Peng, Disentangling the Li-Ion transport and boundary phase transition processes in $Li_{10}GeP_2S_{12}$ electrolyte by In-Operando high-pressure and high-

resolution NMR spectroscopy, Small 19 (2023) 2302863, https://doi.org/10.1002/smll.202302863.
[48] K. Gotoh, M. Maeda, A. Nagai, A. Goto, M. Tansho, K. Hashi, T. Shimizu, H. Ishida, Properties of a novel hard-carbon optimized to large size Li ion secondary battery studied by ^{7}Li NMl, J. Power Sources 162 (2006) 1322–1328, https://doi.org/10.1016/j.jpowsour.2006.09.001.
[49] K. Tatsumi, J. Conard, M. Nakahara, S. Menu, P. Lauginie, Y. Sawada, Z. Ogumi, ^{7}Li NMR studies on a lithiated non-graphitizable carbon fibre at low temperatures, Chem. Commun. (1997) 687–688, https://doi.org/10.1039/A700221A.
[50] J. Okabe, Y. Fang, I. Moriguchi, I. Furó, Structural evolution by heat treatment of soft and hard carbons as Li storage materials: a joint NMR/XRD/TEM/Raman study, J. Mater. Chem. A 13 (2025) 13962–13975, https://doi.org/10.1039/D4TA08096C.
[51] L.M. Bloi, F. Hippauf, T. Boenke, M. Rauche, S. Paasch, K. Schutjajew, J. Pampel, F. Schwotzer, S. Dörfler, H. Althues, M. Oschatz, E. Brunner, S. Kaskel, Mechanistic insights into the reversible lithium storage in an open porous carbon via metal cluster formation in all solid-state batteries, Carbon (2022) 325–335, https://doi.org/10.1016/j.carbon.2021.11.061.
[52] I.E. Gunathilaka, S.A. Ferdousi, F. Chen, M. Armand, A.A.H. Padua, P.C. Howlett, M. Forsyth, L.A. O'Dell, Studying the growth and morphology of metal microstructures in sodium metal batteries with ionic liquid electrolytes by operando ^{23}Na NMR spectroscopy, Nano Energy 133 (2025) 110479, https://doi.org/10.1016/j.nanoen.2024.110479.
[53] D. Cao, T. Ji, A. Singh, S. Bak, Y. Du, X. Xiao, H. Xu, J. Zhu, H. Zhu, Unveiling the mechanical and electrochemical evolution of Nanosilicon composite anodes in sulfide-based all-solid-state batteries, Adv. Energy Mater. 13 (2023) 2203969, https://doi.org/10.1002/aenm.202203969.
[54] N.M. Trease, L. Zhou, H.J. Chang, B.Y. Zhu, C.P. Grey, In situ NMR of lithium ion batteries: bulk susceptibility effects and practical considerations, Solid State Nucl. Magn. Reson. 42 (2012) 62–70, https://doi.org/10.1016/j.ssnmr.2012.01.004.
[55] P. Naillou, A. Boulineau, E.D. Vito, R. Ramos, P. Aza, Evidencing phase transformations of Li_6PS_5Cl argyrodite under ambient air and dry room exposure, ACS Appl. Mater. Interfaces 16 (2024) 53855–53863, https://doi.org/10.1021/acsami.4c11458.
[56] H. Hori, M. Shikano, H. Kobayashi, S. Koike, H. Sakaebe, Y. Saito, K. Tatsumi, H. Yoshikawa, E. Ikenaga, Analysis of hard carbon for lithium-ion batteries by hard X-ray photoelectron spectroscopy, J. Power Sources 242 (2013) 844–847, https://doi.org/10.1016/j.jpowsour.2013.05.160.
[57] N.M. Trease, L. Zhou, H.J. Chang, B.Y. Zhu, C.P. Grey, In situ NMR of lithium ion batteries: bulk susceptibility effects and practical considerations, Solid State Nucl. Magn. Reson. 42 (2012) 62–70, https://doi.org/10.1016/j.ssnmr.2012.01.004.
[58] J.M. Stratford, A.K. Kleppe, D.S. Keeble, P.A. Chater, S.S. Meysami, C.J. Wright, J. Barker, M.M. Titirici, P.K. Allan, C.P. Grey, Correlating local structure and sodium storage in hard carbon anodes: insights from pair distribution function analysis and solid-state NMR, J. Am. Chem. Soc. 143 (2021) 14274–14286, https://doi.org/10.1021/jacs.1c06058.